

Chapter 4

Raman, FTIR and Uv-Visible

In this chapter, the optical and near optical studies are presented. The effect of doping on the local structure of the samples is studied in detail using the Raman and FTIR techniques. The combined results and analysis of the Raman and FTIR measurements are presented in this chapter.

4.1 Raman Study of Pure and doped CuFeO₂

Metal-metal and metal-oxygen bonds directly affect the normal modes of lattice vibrations at the molecular level, which may be responsible for the induced variations in polarizability during the vibrations. In addition, local defects may lead to secondary structures and resultant changes in vibrational modes. Any changes in the normal mode of vibrations and defects can in turn affect the magnetic and electrical properties of the system. Thus, in the present work the investigation has been done for the first time to probe such an aspect particularly for the dopants other than vanadium through Raman spectroscopy measurements.

As already been mentioned earlier, the delafossite has a rhombohedral structure with space group $R\bar{3}m$ and one ABO_2 formula unit per unit cell containing four atoms [1]. This results in zone center having 12 vibrational zones transforming as $\Gamma = A_{1g} + E_g + 3A_{2u} + 3E_u$. Out of which the modes with subscript g are Raman active modes and the other having u are infrared active including acoustic modes $A_{2u} + E_u$ [2]. The “A” mode vibrations are due to Cu-O bonds along the c-axis while the “E” mode vibrations are perpendicular to the c-axis. Only the oxygen atoms vibrate while the Cu and M atoms remain at rest in these modes [3]. Further, it has been proposed by Pellicer-Porres et al. that, the inversion center is lost along the Γ_T direction and the symmetry is reduced from $D3d$ to $C3v$ [2,4,5].

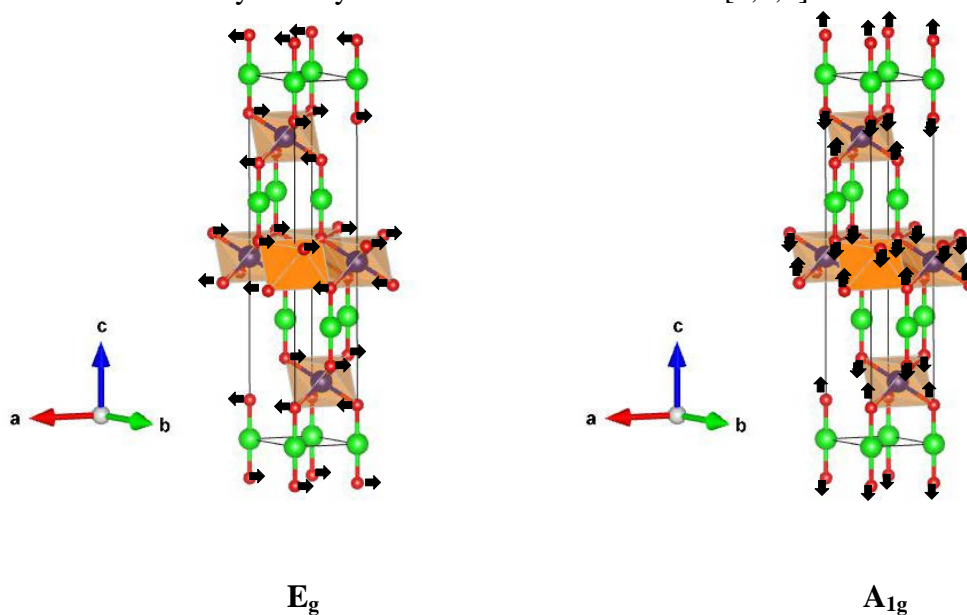


Figure 4.1: E_g and A_{1g} modes of vibration eigen vectors in ABO_2 delafossite compounds

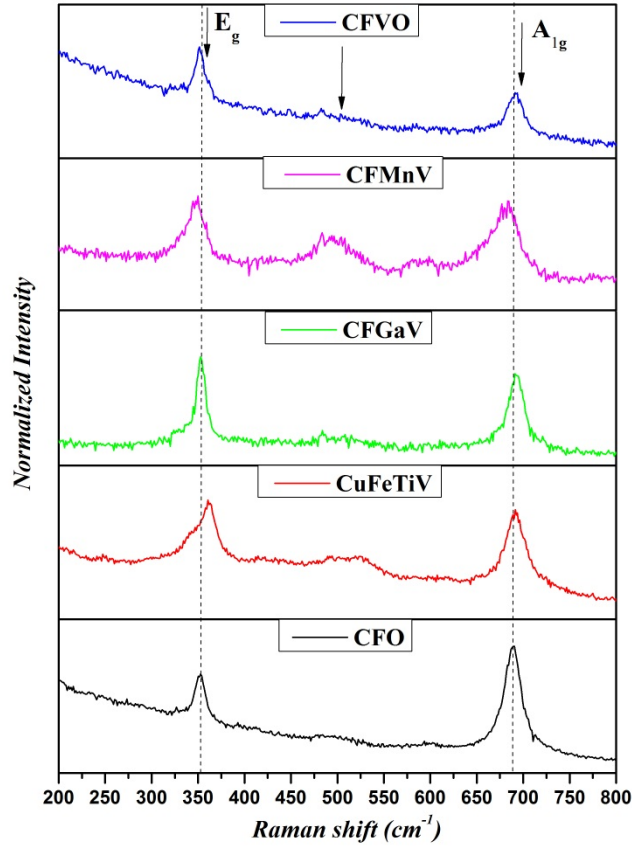


Figure 4.2: Raman plot for pure and doped CuFeO_2 samples

The Raman spectra of pure and doped CuFeO_2 samples are represented in figure 4.2. The typical vibration bands of the samples are seen in the measured spectra [6]. For pure CuFeO_2 samples these bands are observed at $\sigma(E_g) = 352 \text{ cm}^{-1}$ and $\sigma(A_{1g}) = 690 \text{ cm}^{-1}$ [6]. The frequencies of the Raman mode are inversely proportional to the the square root of the reduced mass of vibrating atoms and bond length [3]. Thus, the Raman modes are affected by the change in the Cu-O/M-O bond lengths, reduced mass of MO_6 octahedral and Cu. Substitution at the Fe-site leads to minor changes in the A_{1g} and E_g mode frequencies. The frequencies of both the modes are slightly shifted for CFVO and CFGaV samples and can be ascribed to the minimal changes in the lattice parameters. A Jahn-Teller local distortion attributed broad peak appears around 500 cm^{-1} for pure CuFeO_2 . The intensity for the same peak increases for Ti and Mn-doped samples. To the best of our knowledge, such strong local distortions in the Ti and Mn-doped samples are observed and reported for the first time. Earlier for Ti, Mn and Fe ions at the B-site of ABO_3 having BO_6 octahedra have shown strong Jahn-Teller distortions leading to exquisite magnetic, electrical or multiferroic

properties [7–10]. This could also be the case with modified ABO_2 systems. It has been reported earlier that A_{1g} mode is because of the vibrations of Cu-O bonds along the c-axis, while the E_g mode is due to the vibrations along the a-b plane [3]. The intensity of the A_{1g} mode does not change significantly but there is an evident change in the intensity of E_g mode of the doped samples. This indicates there is an increase in polarization along the a-b plane. Also, the doped samples with Ti show an extra shoulder on the lower wavenumber side of E_g peak apart from the increase in the intensity, suggesting strong distortions in TiO_6 octahedra along the a-b plane. Thus the investigation leads to the confirmation of little or no effect on the basic structure of delafossite due to doping by Ti, Mn, Ga, and V at the Fe site in the decided concentration range. The broadening and the shifting of peaks in the Raman spectra could be explained in terms of the distributions of bond lengths. The unit cells expand due to doping with larger ions which leads to the lower side shifting of the Raman peaks. It should be noted that such local changes are not revealed in the X-ray diffraction patterns, as the reflections are more of long-range order, whereas Raman spectroscopy deals with the local probe of atomic bonding.

The apparent changes in the polarization which is due to the Fe site partial substitutions by unexpected valance state of the dopants, and then the B-site element Fe^{3+} may give rise to the charge fluctuations in Fe. Such changes can be probed through the analysis of Mossbauer resonance which is described in the following section.

4.2 Mossbauer spectroscopy of Pure and doped $CuFeO_2$

The room temperature Mossbauer spectra for pure and doped $CuFeO_2$ samples are shown in the figure 4.3. The paramagnetic nature of the samples is confirmed through the spectra. Quadruple splitting (QS) is observed for both pure and doped samples. Meerwal program was used to carry out least-square fitting of the spectra and the refined Mossbauer parameters are given in table 4.1. The results obtained are in good agreement with earlier reported data for the polycrystalline, single crystals and natural mineral delafossite for pure $CuFeO_2$ sample [11,12].

Fe occupies the expected site in the structure which is confirmed through the results. The values of isomer shift range from 0.37 to 0.39 $mm S^{-1}$ which corresponds to the single high spin Fe^{3+} state present in octahedral oxygen coordination. The presence of Fe^{2+} or mixed valance state at room temperature is disinterested as there is no evidence from the results. The presence of nearly constant values of QS accounts for the asymmetric D_{3d} distortion of the

octahedral [13], where the M atoms are surrounded by oxygen octahedral, which is already reflected earlier in the Raman spectra.

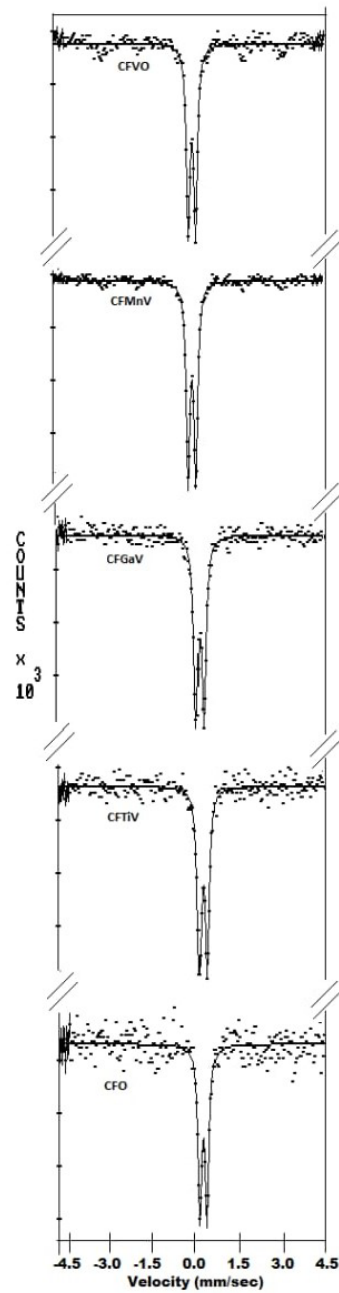


Figure 4.3: Experimental (dots) and calculated (solid line) Mossbauer spectra for CuFeO_2 and doped CuFeO_2 samples obtained at room temperature.

Table 4.1: Mossbauer parameters of the studied samples

Sample	Isomer shift δ (mm s ⁻¹)	QS (mm s ⁻¹)
CFO	0.37	0.61
CFTiV	0.39	0.63
CFMnV	0.39	0.65
CFGaV	0.38	0.62
CFVO	0.38	0.58

4.3 Fourier transformed infrared spectroscopy studies of pure and doped CuFeO₂ samples

As discussed earlier the “A” modes are designated to the movement along with the Cu-O bond directions (i.e. along the c-axis), while the double degenerate “E” modes are attributed to the vibrations along the ab-plane [1]. And only the odd modes “A_u + E_u” are infrared active [1].

The Fourier Transformed Infrared Spectra of pure and doped CuFeO₂ samples are represented in figure 4.4. Strong peak ~ 550 cm⁻¹(shown by arrow) represents metal oxygen bonds showing significant changes due to Ti and Mn doping, supporting our respective observation in Raman Spectra.

The spectra show typical IR bands at 649 cm⁻¹ and 689 cm⁻¹. The results also show the presence of four characteristic bands above 900 cm⁻¹ which are also been reported earlier for the samples of delafossite by Bisbee, Arizona [14,15]. Thus, these along with the above results confirm the single phase of the prepared samples and local distortions in Ti or Mn-doped samples at the Cr-site.

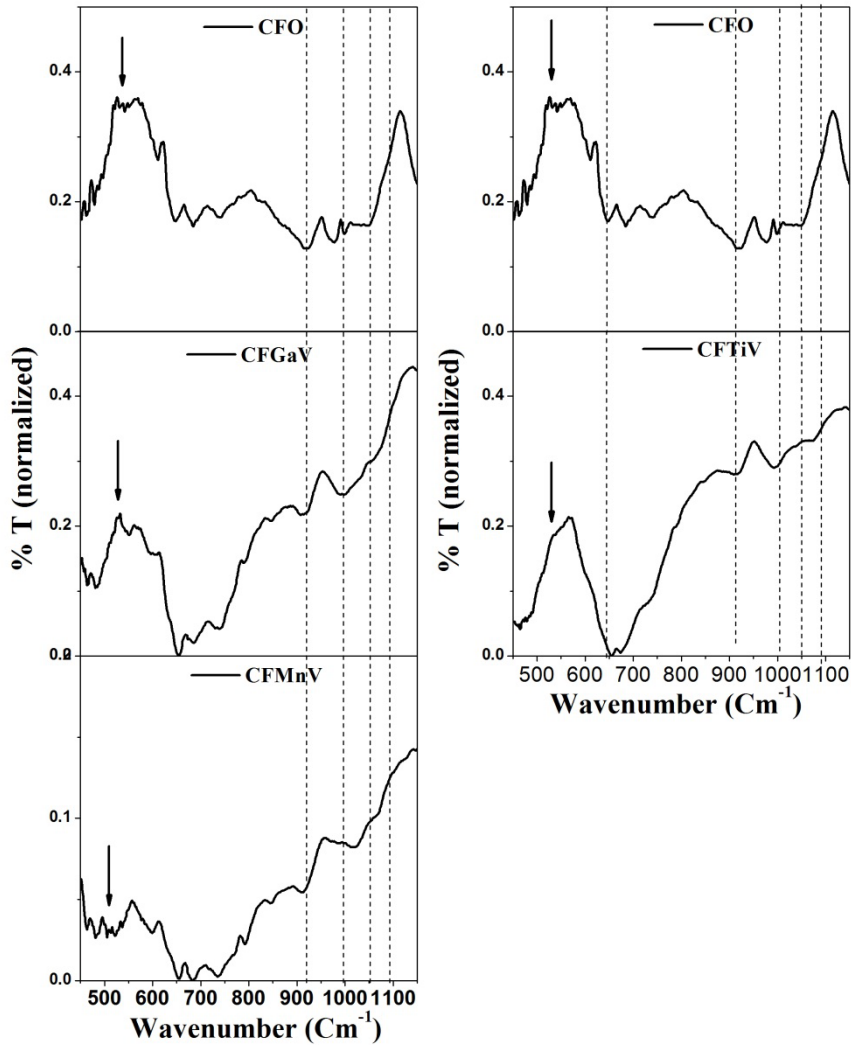


Figure 4.4: FTIR spectra of pure and doped CuFeO_2

4.3 UV-Visible measurements of pure and doped CuFeO_2

As the samples are opaque UV-visible measurements were performed using the diffuse reflectance method using powdered samples. The bandgap was extracted using the Kubelka-Munk (K-M) model explained earlier.

The graph of $[F(R_\infty)hv]^2$ vs hv is given in figure 4.5 and the bandgap of the studied samples was extracted from the intercept on the x-axis. The method of linear regression analysis is used for the same. R^2 is the goodness of fit factor and fitting is performed in the same range (ΔE) of bandgap energy of all the samples. The extracted band gaps are given in table 4.2. From the table, it is clear that there is a minor effect of 4% doping at the B-site of the CuFeO_2 samples.

There are insignificant changes in the optical band gap, but the observed local distortions in Raman and Mossbauer studies have the potential to affect magnetic and electric properties of the doped samples when tested at variable field strengths and temperatures.

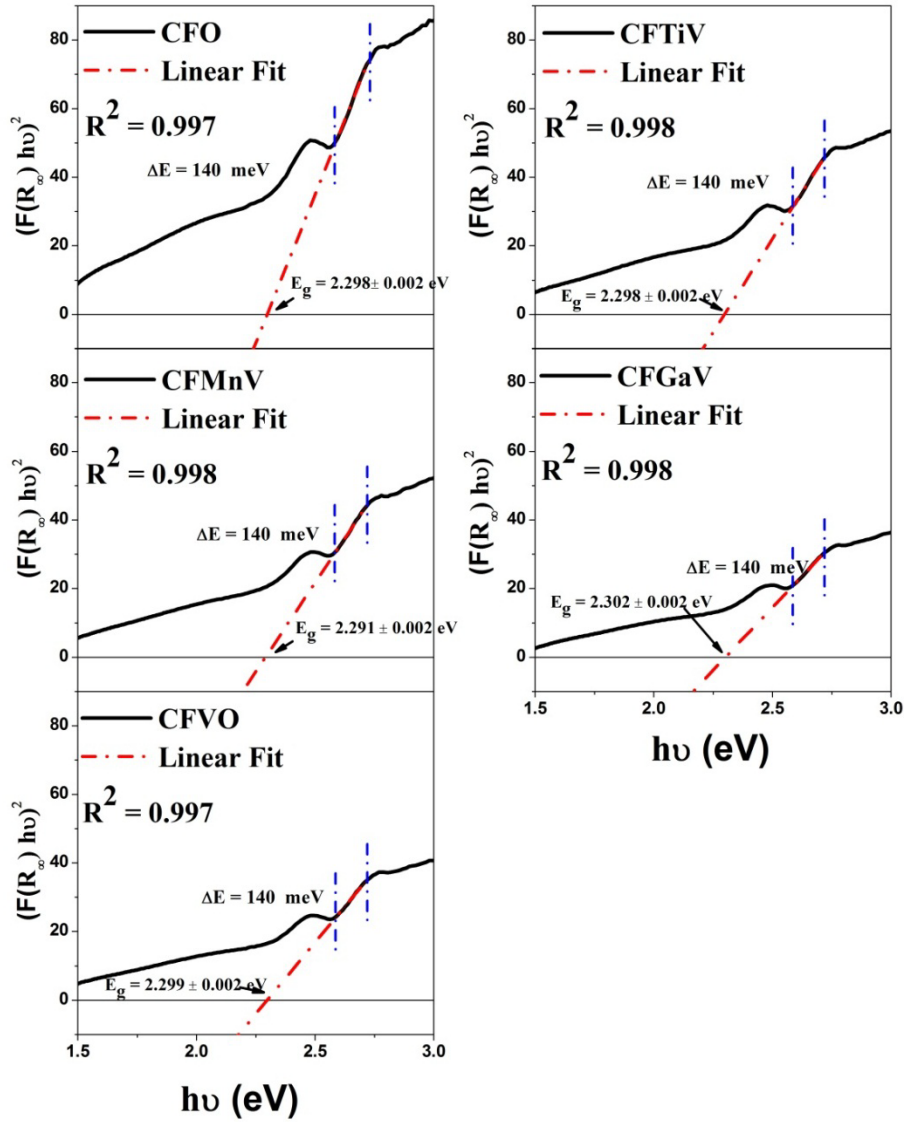


Figure 4.5: K-M transformed reflectance spectra of pure and doped CuFeO_2 samples.

Table 4.2: Observed band gaps in the studied samples

Sample	Bandgap E_g (eV)
CFO	2.298 ± 0.002
CFTiV	2.298 ± 0.002
CFMnV	2.291 ± 0.002
CFGaV	2.302 ± 0.002
CFVO	2.299 ± 0.002

4.4 Raman Study of pure and doped CuCrO₂

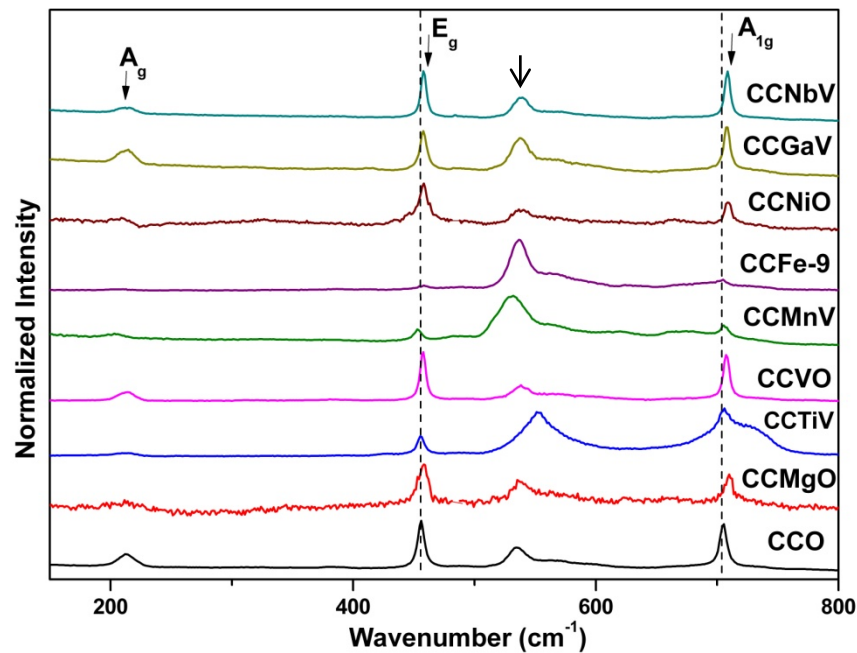


Figure 4.6: Raman spectra of pure and doped CuCrO₂

The ABO₂ structure belongs to the point group C3v and space group R-3 m, which is already been, reported earlier [1]. As discussed “A” mode vibrations are due to Cu-O bonds along the c-axis while the “E” mode vibrations are perpendicular to the c-axis and only the A_{1g} and E_g modes in the CuMO₂ family are Raman active modes [3]. Only the oxygen atoms vibrate while the Cu and M atoms remain at rest in these modes [3]. It has been proposed by Pellicer-Porres et al. that the inversion center is lost along the Γ_T direction and the symmetry is reduced from D3d to C3v [2,4,5].

Raman spectra of pure and doped bulk CuCrO₂ using a 532 nm laser wavelength excitation. On observing the spectra, typical vibrational bands of delafossite structure are seen, as already observed for CuAlO₂[5], CuGaO₂[2] and CuCrO₂[6]. For pure CuCrO₂ the bands are identified as $\sigma(A_{1g})$ at 706 cm⁻¹, $\sigma(E_g)$ at 456 cm⁻¹ and $\sigma(A_g)$ at 213 cm⁻¹ (figure 4.6). As already discussed before, the changes in the Cu-O/M-O bond lengths and also the reduced mass of Cu and MO₆ octahedra do affect the Raman modes of vibrations [2]. It is clearly seen that there are minute changes in the frequencies of A_{1g} and E_g modes due to doping. This is also justified by the minor changes in the Cu-O and M-O bonds lengths observed in chapter 3. A broad band structure, attributed to the presence of local distortions, can be observed near 535 cm⁻¹, for the pristine and doped CuCrO₂[6]. A strong local distortion in Mn, Ti, and Fe doped samples have been observed for the first time, which are contrary to the earlier reports. The presence of Ti, Mn and Fe ions at the B-site in the ABO₃ system forming the

BO₆ octahedra along with the possibility of mix or higher valence at the B-site atom leads to strong Jahn-Teller distortions is also well-known [7–10]. This in turn results in exotic magnetic and electrical properties in this class of compounds. The exchange interactions between the magnetic cations are directly affected by the structural geometry of the triangular planar lattice [16]. Similar scenarios could be plausible in the present case of the modified ABO₂ systems.

Magnitude is reversed for the A_{1g}-E_g modes in the case of Mn, Fe, Ti and Ga doped samples. This is attributed to the local distortions induced changes in the polarization along the ab plane or/ and along the c-axis in these doped samples. Apart from the enhanced intensity of A_{1g} mode at the expense of E_g, Ti-doped samples show an additional strong shoulder on the higher wavenumber side of A_{1g} peak. Such modification points out strong distortions in the TiO₆ octahedra parallel to the c-axis. Such effects are likely to affect the electronic bandgap structure of these doped samples, which in turn, may affect the magnetic and electric properties of these multi-functional oxide systems.

4.5 Fourier transformed infrared spectroscopy studies of pure and doped CuCrO₂ samples

Figure 4.5 represents the infrared spectra of pure and doped CuCrO₂ samples. We observed several sharp peaks at wave numbers ~742, ~944, ~1048 and ~1122 cm⁻¹ and a broad peak between 490-600 cm⁻¹. The peaks between 400 to 600 cm⁻¹ are associated with E_u mode, while the peak around 700 cm⁻¹ is associated with A_{2u} mode, which is already predicted through the ab initio calculations [1]. Absorption peaks between 550-600 cm⁻¹ are attributed to Cu-O stretching and O-Cu-O asymmetric stretching, while the peaks between 700-800 cm⁻¹ are assigned to Cr/M-O stretching vibrations in distorted CrO₆ octahedra [17]. The O-O stretching vibrations are represented by peaks between 900-1100 cm⁻¹ which in our measurements show minute changes.

The possibility of O atoms vibrating in opposite directions, have been predicted through group-theory analysis, producing IR absorptions, as suggested by Pellicer-Porres et al. [2]. The frequencies of transverse (T_o) and longitudinal (L_o) optical modes within E_u and A_{2u} modes were obtained by them through ab initio calculations. But the evidence for the distinct presence of T_o and L_o modes within E_u and A_{2u} modes wasn't found by them in CuGaO₂ samples [2]. Clear splitting of the E_u and A_{2u} modes in the doped CuCrO₂ samples was importantly observed by us (figure 4.7), where Cr is partially substituted by V, Ga, Nb, Ti and Mn ions. No splitting was observed in pristine, Ni and Fe doped CuCrO₂ samples. the

present observations suggests that the asymmetrical stretching vibrations, i.e parallel as well as perpendicular to c-axis, leads to the removal of the degeneracy in optical modes of vibrations for the V, Ga, Nb, Ti and Mn-doped samples. Also, the possibility of the higher valance induced electron doping might be responsible for changes in the local dipole moments and in turn, lead to the removal of the degeneracy of optical modes of vibrations in these doped samples. Thus, the valance states of V, Nb, Ti, or Mn when substituted at the Cr site are expected to be higher than 3+ in these samples. A similar kind of L_o/T_o doping was observed in $CuCrO_2$ earlier but due to temperature variations [16]. The unit cell is significantly polarized by the A_{2u} mode and causes the L_o/T_o splitting. The intrinsic correlation between the optical and magnetic transitions for $CuCrO_2$ was held responsible for such L_o/T_o splitting [16].

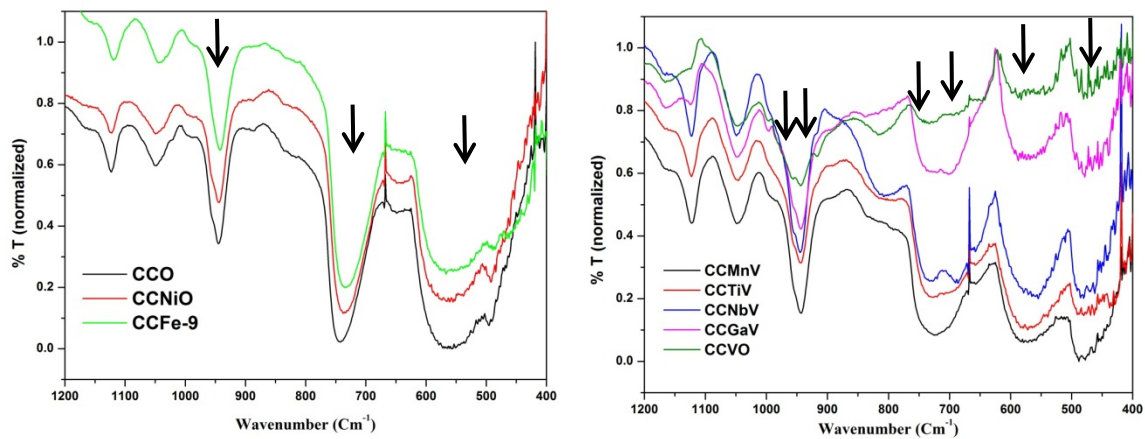


Figure 4.7: FTIR spectra of pure and doped $CuCrO_2$

4.6 Uv-Visible measurements of pure and doped $CuCrO_2$

The above-observed changes in the local polarizations/dipole moments and crystal structure can lead to changes in the electronic structure related physical. Thus, an optical band study is performed at room temperature for all the samples. As already discussed these samples being opaque the extraction of the direct bandgap is done through Uv-visible measurements in reflectance mode. The band gaps were determined using the diffuse reflectance data through the K-M model.

Figure 4.8 and 4.9 shows the plots between $[F(R_\infty)hv]^2$ and hv , from which direct band gaps of the samples were extracted. Respective bandgaps of the studied samples are extracted from the interception at the x-axis using the linear regression analysis, R^2 is the goodness of fit factor and fitting is performed almost within the same range (ΔE) of bandgap energy for all the compositions. The bandgap values are presented in table 4.3.

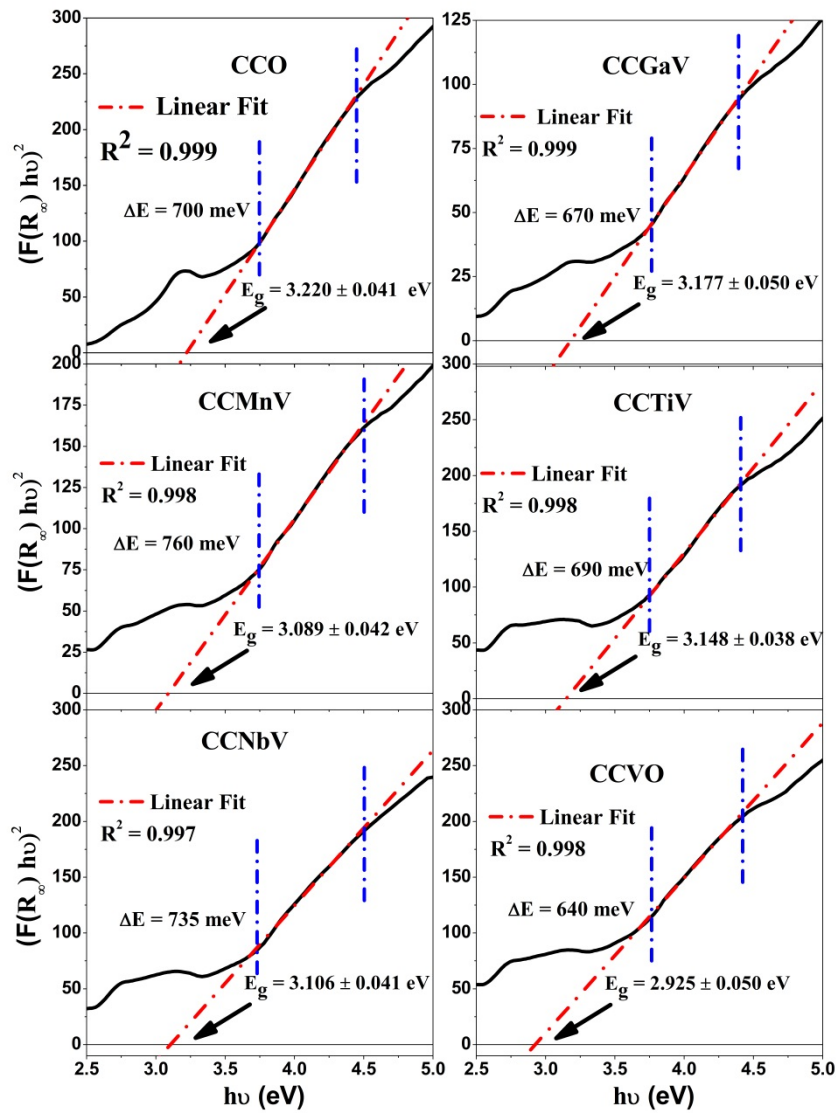


Figure 4.8: Kubelka-Munk transformed reflectance spectra of CuCrO_2 , $\text{CuCr}_{0.96}\text{M}_{0.03}\text{V}_{0.01}\text{O}_2$ ($\text{M} = \text{Ti, Mn, Ga, and Nb}$), and $\text{CuCr}_{0.96}\text{V}_{0.04}\text{O}_2$ samples.

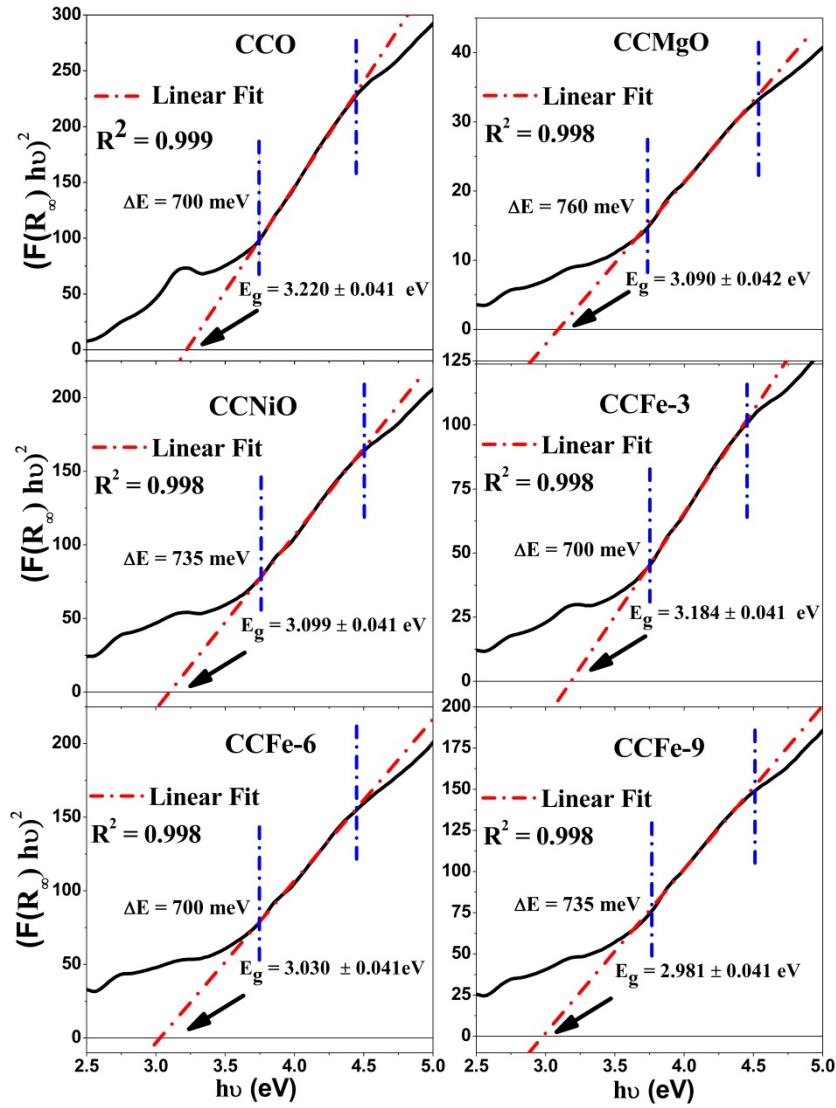


Figure 4.9: Kubelka-Munk transformed reflectance spectra of CuCrO_2 , $\text{CuCr}_{1-x}\text{Fe}_x\text{O}_2$ ($x = 0.03, 0.06, \text{ and } 0.09$), $\text{CuCr}_{0.97}\text{Mg}_{0.03}\text{O}_2$, and $\text{CuCr}_{0.97}\text{Ni}_{0.03}\text{O}_2$ samples.

Table 4.3: Observed bandgaps in the studied samples

Electron doped Samples		Hole doped Samples	
Sample	Bandgap E_g (eV)	Sample	Bandgap E_g (eV)
CCO	3.220 ± 0.041	CCO	3.220 ± 0.041
CCGaV	3.177 ± 0.050	CCMgO	3.090 ± 0.042
CCMnV	3.089 ± 0.042	CCNiO	3.099 ± 0.041
CCTiV	3.148 ± 0.038	CCFe-3	3.184 ± 0.041

No significant changes were observed in the respective direct bandgaps when doped by iso-valent cation, i.e., Ga^{3+} (same valence as that of Cr^{3+}). On the other hand, when doped at the trivalent Cr-site with either mixed/or tetravalent ions (i.e., $\text{Mn}^{3+/4+}$ and Ti^{4+}) as well as penta-valent Nb^{5+} , the bandgap reduces (see Table 4.3). Further, the pristine CuCrO_2 compound is known to have hole carriers, doping with ions having valence with 2+/3+ mixed (Fe) or 2+ valence (such as Mg and Ni) found to reduce the bandgap. A maximum reduction in the bandgap from 2.981 to 2.925 eV was obtained for doping by either Fe(9%) or V(4%). We reported earlier some changes in the M-O, Cr-O, and Cu-O bond distances, unit cell volumes and crystallite size for these dopants, but found no direct correlation with respective bandgaps [18]. The earlier studies indicate that the effect of doping in CuCrO_2 is most likely attributed to the changes in *p-d* hybridizations coupled with the Jahn-Teller distortions, leading to the observed reductions in the gap between the top of the valence band and the bottom of the conduction band [18–22].

It is noted that the electron doping could lead to partial compensation of holes that might result in an increase in electrical resistivity, as both electrons and holes contribute to the electrical transport resulting in the decreased electrical resistivity. On the other hand, the addition of holes by mixed-valence doping of 2+ and 3+, or 2+ ions could lead to a reduction in electrical resistivity. Further, local distortions, due to the above spectrum of dopants, as well as their doping levels, are too complex to have a direct correlation with measured physical properties. Nevertheless, the changes induced by hole doping mediated by superexchange coupling or double exchange between the Cr-O-M-O linkages are likely to have direct bearings on the transport, magnetic, and electrical properties of $\text{CuCr}_{1-x}\text{M}_x\text{O}_2$ compounds [23–25], in particular as a function of temperature. Such a study is discussed in the preceding chapters.

4.7 Conclusions

Following conclusions can be drawn from the above studies:

- Room-temperature Raman studies of pure and doped CuFeO_2 samples showed a minor shift in peaks due to E_g and A_{1g} modes for Ti and Mn-doped samples. Moreover, all the samples exhibited induced extra peak around 500 cm^{-1} due to local Jahn–Teller distortion but with variable strength. The presence of octahedron distortion was confirmed through the values of quadrupole splitting obtained from the room-temperature Mössbauer measurements. The absence of Fe^{2+} or mix valence was also suggested by the

Mössbauerspectra. The FTIR studies along with the Raman, Mossbauer and X-ray diffraction studies earlier confirm the phase purity of these samples prepared through the cost-effective solid-state technique with high vacuum-sealed annealing, rather than heating under inert atmosphere provided through inert gases. No significant changes in the optical band gap are observed for the pure and doped CuFeO_2 samples.

- The observed changes discussed earlier for the pure and doped CuCrO_2 samples through the values of lattice parameters, bond distances and/or bond angle are found to correlate more with the local electronic structure and local crystal structure rather than ionic size. Significantly strong local distortions, not been reported earlier, were observed in Mn, Ti and Fe doped CuCrO_2 compounds through Raman studies. Additionally, removal of degeneracy is observed, related to the transverse (T_o) and longitudinal (L_o) optical modes of vibrations, in both E_u and A_{2u} IR active modes. This is presumably due to the higher valence state induced electron doping which in turn changes the local dipole moments in the CuCrO_2 compounds. The optical bandgap of CuCrO_2 was found to reduce by either mixed/or di- or tetra-valent ions doping at the trivalent Cr-sites. A maximum reduction in bandgap from 2.981 to 2.925 eV was obtained for doping by either Fe (9%) or V (4%). It is revealed that the changes in M-O, Cr-O, Cu-O bond distances, unit cell volumes, or crystallite size in these doped samples have no direct correlation with respective bandgaps. Instead, the changes in the $p-d$ hybridizations coupled with the Jahn Teller distortions might be the cause of the observed reductions in the bandgap.

References

- [1] S.P. Pavunny, A. Kumar, R.S. Katiyar, Raman spectroscopy and field emission characterization of delafossite CuFeO_2 , *J. Appl. Phys.* 107 (2010). <https://doi.org/10.1063/1.3284160>.
- [2] J. Pellicer-Porres, A. Segura, E. Martínez, A.M. Saitta, A. Polian, J.C. Chervin, B. Canny, Vibrational properties of delafossite CuGaO_2 at ambient and high pressures, *Phys. Rev. B - Condens. Matter Mater. Phys.* 72 (2005). <https://doi.org/10.1103/PhysRevB.72.064301>.
- [3] N.P. Salke, K. Kamali, T.R. Ravindran, G. Balakrishnan, R. Rao, Raman spectroscopic studies of CuFeO_2 at high pressures, *Vib. Spectrosc.* 81 (2015) 112–118. <https://doi.org/10.1016/j.vibspec.2015.10.010>.
- [4] J. Pellicer-Porres, A. Segura, C. Ferrer-Roca, D. Martínez-García, J.A. Sans, E. Martínez, J.P. Itié, A. Polian, F. Baudalet, A. Muñoz, P. Rodríguez-Hernández, P. Munsch, Structural evolution of the CuGaO_2 delafossite under high pressure, *Phys. Rev. B - Condens. Matter Mater. Phys.* 69 (2004). <https://doi.org/10.1103/PhysRevB.69.024109>.
- [5] J. Pellicer-Porres, D. Martínez-García, A. Segura, P. Rodríguez-Hernández, A. Muñoz, J.C. Chervin, N. Garro, D. Kim, Pressure and temperature dependence of the lattice dynamics of CuAlO_2 investigated by Raman scattering experiments and ab initio calculations, *Phys. Rev. B - Condens. Matter Mater. Phys.* 74 (2006). <https://doi.org/10.1103/PhysRevB.74.184301>.
- [6] O. Aktas, K.D. Truong, T. Otani, G. Balakrishnan, M.J. Clouter, T. Kimura, G. Quirion, Raman scattering study of delafossite magnetoelectric multiferroic compounds: CuFeO_2 and CuCrO_2 , *J. Phys. Condens. Matter.* 24 (2012). <https://doi.org/10.1088/0953-8984/24/3/036003>.
- [7] S. Lenjer, O.F. Schirmer, H. Hesse, T.W. Kool, Conduction states in oxide perovskites: Three manifestations of (formula presented) Jahn-Teller polarons in barium titanate, *Phys. Rev. B - Condens. Matter Mater. Phys.* 66 (2002) 1–12. <https://doi.org/10.1103/PhysRevB.66.165106>.
- [8] H. Yabuta, H. Tanaka, T. Furuta, T. Watanabe, M. Kubota, T. Matsuda, T. Ifuku, Y. Yoneda, Enhancement of tetragonal anisotropy and stabilisation of the tetragonal phase by Bi/Mn-double-doping in BaTiO_3 ferroelectric ceramics, *Sci. Rep.* 7 (2017).

- <https://doi.org/10.1038/srep45842>.
- [9] J. Fridrichová, P. Bačík, A. Ertl, M. Wildner, J. Dekan, M. Migliorini, Jahn-Teller distortion of Mn^{3+} -occupied octahedra in red beryl from Utah indicated by optical spectroscopy, *J. Mol. Struct.* 1152 (2018) 79–86. <https://doi.org/10.1016/j.molstruc.2017.09.081>.
- [10] D.D. Shah, P.K. Mehta, M.S. Desai, C.J. Panchal, Origin of giant dielectric constant in $Ba[(Fe_{1-x}Co_x)_{1/2}Nb_{1/2}]O_3$, *J. Alloys Compd.* 509 (2011) 1800–1808. <https://doi.org/10.1016/j.jallcom.2010.10.045>.
- [11] A. Mary Sukeshini, H. Kobayashi, M. Tabuchi, H. Kageyama, Physicochemical characterization of $CuFeO$ and lithium 2 intercalation, 2000. www.elsevier.com/locate/ssi.
- [12] A.H. Muir, H. Wiedersich, An investigation of $CuFeO_2$ by the Mössbauer effect, *J. Phys. Chem. Solids.* 28 (1967) 65–71. [https://doi.org/10.1016/0022-3697\(67\)90198-9](https://doi.org/10.1016/0022-3697(67)90198-9).
- [13] K. El Ataoui, J.P. Doumerc, A. Ammar, L. Fournès, A. Wattiaux, J.C. Grenier, M. Pouchard, Mössbauer study and magnetic properties of $CuFe_{1-x}Ga_xO_2$, *J. Alloys Compd.* 368 (2004) 79–83. <https://doi.org/10.1016/j.jallcom.2003.09.003>.
- [14] A.F. Rogers, Delafossite, a cuprous metaferrite from Bisbee, Arizona, *Am. J. Sci.* s4-35 (1913) 290–294. <https://doi.org/10.2475/AJS.S4-35.207.290>.
- [15] M. Roble, S.D. Rojas, R. Wheatley, S. Wallentowitz, A.L. Cabrera, D.E. Diaz-Droguett, Hydrothermal improvement for $3R-CuFeO_2$ delafossite growth by control of mineralizer and reaction atmosphere, *J. Solid State Chem.* 271 (2019) 314–325. <https://doi.org/10.1016/J.JSSC.2019.01.014>.
- [16] X. Li, J. Wang, J. Zhang, Y. Li, Z. Hu, J. Chu, Spin-manipulated phonon dynamics during magnetic phase transitions in triangular lattice antiferromagnet $CuCr_{1-x}Mg_xO_2$ semiconductor films, *RSC Adv.* 6 (2016) 27136–27142. <https://doi.org/10.1039/c6ra02881k>.
- [17] A.N. Banerjee, S. Kundoo, K.K. Chattopadhyay, Synthesis and characterization of p-type transparent conducting $CuAlO_2$ thin film by DC sputtering, *Thin Solid Films.* 440 (2003) 5–10. [https://doi.org/10.1016/S0040-6090\(03\)00817-4](https://doi.org/10.1016/S0040-6090(03)00817-4).
- [18] N. Barot, P.K. Mehta, A. Rao, R. Thomas, Y.-K. Kuo, Effects of iso- and polyvalent substitutions on the short/long-range crystalline order in $CuCrO_2$ compounds, *J. Alloys Compd.* 791 (2019). <https://doi.org/10.1016/j.jallcom.2019.03.291>.
- [19] T. Elkhouni, M. Amami, C. V. Colin, A. Ben Salah, Structural and magnetoelectric

- interactions of (Ca, Mg)-doped polycrystalline multiferroic CuFeO_2 , *Mater. Res. Bull.* 53 (2014) 151–157. <https://doi.org/10.1016/j.materresbull.2014.01.035>.
- [20] J. Wang, P. Zhang, Q. Deng, K. Jiang, J. Zhang, Z. Hu, J. Chu, Electronic transitions of the transparent delafossite-type $\text{CuGa}_{1-x}\text{Cr}_x\text{O}_2$ system: first-principles calculations and temperature-dependent spectral experiments, *J. Mater. Chem. C* 5 (2016) 183–191. <https://doi.org/10.1039/C6TC04535A>.
- [21] F. Lin, W. Shi, A. Liu, Optical bandgap modulation and magnetic characterization of Fe-doped CuCrO_2 nanopowders, *J. Alloys Compd.* 529 (2012) 21–24. <https://doi.org/10.1016/j.jallcom.2012.03.059>.
- [22] F. Lin, C. Gao, X. Zhou, W. Shi, A. Liu, Magnetic, electrical and optical properties of p-type Fe-doped CuCrO_2 semiconductor thin films, *J. Alloys Compd.* 581 (2013) 502–507. <https://doi.org/10.1016/J.JALLCOM.2013.07.160>.
- [23] D. Li, X. Fang, W. Dong, Z. Deng, R. Tao, S. Zhou, J. Wang, T. Wang, Y. Zhao, X. Zhu, Magnetic and electrical properties of p-type Mn-doped CuCrO_2 semiconductors, *J. Phys. D: Appl. Phys.* 42 (2009). <https://doi.org/10.1088/0022-3727/42/5/055009>.
- [24] T. Elkhouni, M. Amami, C. V. Colin, P. Strobel, A. Ben Salah, The structure, Raman spectroscopy and evidence of ferromagnetic transition in $\text{CuCr}_{1-x}\text{M}_x\text{O}_2$ ($\text{M}=\text{Mn}$ and Rh) compounds, *J. Magn. Magn. Mater.* 355 (2014) 158–163. <https://doi.org/10.1016/J.JMMM.2013.12.004>.
- [25] T. Elkhouni, M. Amami, P. Strobel, A. Ben Salah, Structural and Magnetic Properties of Substituted Delafossite-Type Oxides CuCrO_2 , *World J. Condens. Matter Phys.* 03 (2013) 1–8. <https://doi.org/10.4236/wjcmp.2013.31001>.